Assessment of Quantum Mechanical Models Based on Resolved Orbital Momentum Distributions of *n*-Butane in the Outer Valence Shell

Feng Wang*

Centre for Molecular Simulation, Swinburne University of Technology, Hawthorn, Melbourne, Victoria 3122, Australia

Received: August 12, 2003; In Final Form: September 29, 2003

Fully resolved outer valence orbital momentum distributions (MDs) of *n*-butane (C_4H_{10}) in the ground electronic state (X^1A_g) are studied quantum mechanically using RHF/TZVP, density functional theory (DFT) DFT-BP/TZVP, and B3LYP/TZVP methods. The orbital MDs are simulated to reflect the recent experimental conditions with the plane wave impulse approximation (PWIA) and are compared favorably with the available experimental orbital cross sections. However, the majority of the outer valence molecular orbitals (MOs) of *n*-butane has been only partially resolved experimentally, forming into three clustered MOs of $7a_g + 2b_g + 6a_g$, $2a_u + 6b_u$ and $1b_g + 5b_u + 5a_g$. Deconvolution of the clustered MOs is a challenge experimentally but rather straightforward theoretically, as the inversion is a multiple channel process. The outer valence MOs are crucial to understanding the chemical bonding mechanism and the unresolved outer valence orbitals cause significant bonding information loss. This work provides an orbital based assessment to the quality of the RHF/TZVP, DFT-BP/TZVP, and B3LYP/TZVP models using orbital MD information, by decomposing the clustered outer valence MOs of *n*-butane, which also reveals the bonding mechanism of the species.

I. Introduction

Electron momentum spectroscopy (EMS) is a unique technique in molecular spectroscopy because it measures the binding energies which are directly mapped to the square of the orbital wave functions through orbital MDs. Energy and its wave function are the core of quantum mechanics (QM). However, unlike the energy, the quality of the wave function was usually assessed indirectly through related molecular properties until the EMS orbital MDs became available. Molecular orbitals are the primary description of the electronic structure of molecules and play a central role in the understanding of all aspects of chemical phenomena.[1] Molecular orbital theory concentrates on the valence-shell of molecules for the chemical bonding mechanism, as electrons in the core-shell of an atom are less sensitive to their environment than are the valence electrons. The valence orbitals of a molecule can be directly measured only by the EMS through orbital momentum distributions at present.

Butane is a simple saturated hydrocarbon alkane composed of four carbon atoms and connected only by single bonds. It is one of the simplest alkane compounds which have attracted considerable research attention experimentally and theoretically in the past few decades. Some good summaries of previous research in butane are given in refs 2 and 3. Until recently, the structure of simple alkane was thought fully understood, leading to conclusions such as "the classification of the valence molecular orbitals of a C_nH_{2n+2} alkane into *n* inner valence levels in the C_{2s} region, well separated from the $n + 2$ outer molecular orbitals of dominant $C_{2p} + H_{1s}$ character". Such a conclusion has been seriously challenged by EMS experiments of *n*-butane ($CH_3CH_2CH_2CH_3$). Despite the apparent simplicity, butane is also complex enough to possess both constitutional and conformational isomers, with low rotational energy barriers on the *n*-butane potential energy surface and with small orbital energy splitting in the outer valence shell. The low energy barriers that resulted in free C−C rotational and torsional motions under the experimental condition can cause some orbital cross sections being trapped into the local energy minimum structure of butane[6,7] in the experiment. Nevertheless, the small orbital energy splitting in either *n*-butane[5] or isobutane[8,9] brings great challenges to the modern EMS technique and leads to partially resolved orbital momentum distributions, causing information loss in the chemically most significant region. Some recent EMS analysis, such as for *n*-butane,[3,4] employed high-level theoretical methods *separately* for the binding energies and orbital MDs. For example, the Green function calculations with various basis sets such as 1p-GF/ADC(3)/6-311G**[3] are used for the binding energies and B3LYP/6-311++G**[3] for the orbital cross section simulations of *n*-butane. Unfortunately, the *n*-butane binding energies were decoupled from their orbital MDs, which virtually demolishes the significance of the EMS technique as a unique tool of detecting both energy and wave function simultaneously. Furthermore, the 1p-GF/ADC(3) method does not provide a direct orbital-based mapping into the B3LYP orbital wave functions.[3] As a result, there is no guarantee that the 1p-GF/ADC(3) and B3LYP methods are dealing with the same molecular orbitals.

Careful design and consideration for both theoretical and experimental studies are required to reveal the subtle differences of chemical bonds caused by the environment effects of the elements. It is beyond the reach of many QM models in configuration space, which are dominated by the energy of the molecular equilibrium structure and its wave function that is usually determined by energy minimization.[1] In most cases, molecular wave functions so-obtained emphasize the isotropy (radial dependence) rather than the anisotropy (angular dependence) in the configuration space. For example, many post-HF methods, such as MP2, largely concentrate on electronic

* To whom correspondence should be addressed.

10.1021/jp0363904 CCC: $25.00
Published on Web 11/04/2003

energies, which cause significant losses either in the capability (e.g., MP2) to predict properties other than the total energy, such as dipole moments, as MP2 provides only self-consistent field (SCF) wave functions in most of the computational chemistry packages such as Gaussian 03 or losses the simple molecular orbital picture (e.g., CI), as the MO wave functions become a mixture of weighted configurations unless full CI is achieved. Nevertheless, quantum mechanics does not automatically guarantee the angular behavior of the electronic wave functions particularly in the long-range regions.[10] Due to the isotropic nature of the wave function generation, improvement in the angular behavior of wave functions usually does not lead to significant improvement in total electronic energy. In the configuration space, there does not exist any efficient descriptions to assess the quality of orbital wave functions directly, and the energetic properties, therefore, become the dominant measures of quality assessment for a QM model.

Molecular orbital wave functions in momentum space, such as orbital MDs, provide quantitative and detailed structural information on the anisotropy of wave functions in the entire region with emphasis on the long range. Therefore, orbital MDs are capable of providing direct assessment and indication of the angular dependence in the chemical bonding mechanism, which is particularly responsible for phenomena such as organic molecular isomerization, bond angles, and wave function anisotropy. As a continuous study of the *n*-butane valence orbitals,[6,7] this paper provides comprehensive QM orbital MD simulations of the individual outer valence orbitals for normal butane. A group of well designed QM models, such as RHF, B3LYP, and density functional theory (DFT) using generalized gradient approximation (GGA) with exchange-correlation (XC) energy due to Becke[11] and Perdew[12] (DFT-BP) are employed, together with the DGauss valence polarized triplet zeta basis set (TZVP).[13] The TZVP basis set, which is specifically designed for DFT calculations,[13] together with the DFT-BP model, agrees well with EMS orbital MDs to the experiment for a number of organic compounds,[14−19] so that it is employed in this study for the calculations in order to minimize basis set related errors. Comparison between the orbital MDs using different QM models, along with available experiment, on an individual MO base will not only provide information regarding the electronic structures of the molecule but it also provides theoretical insight of the approximations on which the models are based. Furthermore, as the energy resolution of high-resolution EMS spectrometer available is 0.52 eV,[19] the chemically most important outer valence orbital energies of *n*-butane could not be fully resolved by the experiment.[5] The present study therefore provides fully resolved orbital MDs for the outer valence MOs of *n*-butane in the region of 11−16 eV, to explore information beyond the reach of the experiment.

We begin our discussion by comparing orbital energies of the molecule calculated using various QM models with experiments. The outer valence orbital MDs are simulated individually and compared collectively with the available experiment. The individual orbital MDs are presented and discussed in the next section, focusing on the assessment of orbital based XC energy included in the QM models as well as the complexities of the HOMO and NHOMO. Finally, conclusions from the present work are drawn.

II. Computational Details and Orbital Energies of *n*-Butane

The ground electronic state (X^1A_g) of *n*-butane with point group symmetry C_{2h} is considered in this work. The molecule orientation in space is the same as mentioned elsewhere. The configuration of *n*-butane with C_{2h} symmetry is the global energy minimum structure on the potential energy surface formed by its conformational isomers of the torsional motions of the butane central carbon C−C bond.[6,7] The four carbon atoms are connected by single bonds, and the carbon atoms are numbered as $C_{(3)}-C_{(1)}-C_{(2)}-C_{(4)}$. The *Z*-shaped carbon nuclei framework is confined in the *xy* plane, and the C_2 rotational axis coincides with the *z* axis in space.

TABLE 1: Comparison of the Molecular Geometry of *n*-Butane (C_4H_{10}) Produced Using Quantum Mechanical Calculations

geometries	RHF/TZVP	DFT-BP/TZVP	B3LYP/TZVP
C_1-C_2/Å	1.529	1.511	1.533
C_1-C_3/Å	1.528	1.512	1.530
C_1-H_{11}/Å	1.088	1.108	1.096
C_3-H_5/Å	1.086	1.104	1.093
C_3-H_7/Å	1.086	1.105	1.094
$C_3-C_1-C_2$/°	113.142	113.135	113.306
$H_{11}-C_3-H_{13}$/°	106.269	105.658	106.001
$H_9-C_3-H_7$/°	107.675	107.177	107.503
$H_5-C_1-H_7$/°	107.763	107.660	107.649
$H_{11}-C_1-C_2$/°	109.215	108.829	109.518
total energy/E_h	−157.338015	−158.497078	−158.387820

The electronic calculations are performed using the RHF/TZVP, DFT-BP/TZVP, and B3LYP/TZVP models with energy minimization. The same TZVP basis set is used in all models in order to minimize the basis set related errors hereby to ensure comparison between the QM models. The *n*-butane molecular point group symmetry of C_{2h} is imposed in the electronic structure calculations using the GAMESS02 suite of programs[20] to reduce computation and to ensure orbital symmetry, except for the DFT-BP/TZVP calculations which used the DGauss suite of programs.[21,22] The total electronic energy of *n*-butane in the ground electronic state is given by −157.338015, −158.497078, and −158.387820 E_h using RHF/TZVP, DFT-BP/TZVP, and B3LYP/TZVP models, respectively, with individual geometry optimization. Note that all wave functions are generated from separate single-point calculations at the optimized geometries using the same models, such as RHF/TZVP(single-point)//RHF/TZVP(optimization), to minimize the errors in the wave functions caused by the optimization calculations. Because in GAMESS02,[20] like most other quantum mechanical packages, a geometry optimization calculation is terminated when the total electronic energy converges (to a given criterion), as a result, the total energy is calculated at the *n*th step, whereas the wave functions and many other properties are calculated at the previous $(n-1)$th step. As the energy converges, $E_n = E_{(n-1)}$, but this does not guarantee the *n*th and $(n-1)$th wave functions are the same, in particular, when the wave functions are very anisotropic. Consequently, a single-point energy calculation is needed to ensure that the wave functions are produced at the exactly optimized molecular geometry.

Table 1 lists the optimized geometries of *n*-butane obtained using these QM models. As indicated in this table, all of the predicted geometries of the molecule are consistent. As expected, the optimized bond lengths by the QM models agree generally better than the bond angles, mainly due to the isotropic nature of the models employed. The fact that different C−C and C−H bond lengths exhibit subtle differences indicates that those bonds in *n*-butane are not identical as a result of the element environment (or symmetry) effects. Therefore, to claim, as is stated in many organic chemistry textbooks, that all of the C−H bonds and C−C bonds in *n*-butane are the same is only approximately valid. However, some properties such as disper-

sion forces, dipole moments, and orbital anisotropy can only be understood when anisotropic structural information is taken into account.[23] Bond angles are of importance with respect to the chemical bonding mechanism as they directly determine the bond fashion such as the σ or π bond. In Table 1, the agreement on bond angles between the QM models is not as good as for the bond lengths, though they are consistent. This is an indicator of capability for the QM models to produce the orbital wave function anisotropy, which may be presented qualitatively through the orbital electron density contour plots in space. However, a more detailed and quantitative assessment of orbital wave function anisotropy of a molecule can only be achieved by orbital momentum distributions so far.

Valence shell orbital symmetry classification for *n*-butane is determined by the point group symmetry of the orbital wave functions as well as the orbital energies and their ordering. In the outer valence shell, the orbital energies and their ordering often depend on the model employed due to the small orbital energy splitting. For example, ref 4 gives the outer valence configuration for *n*-butane of C_{2h} symmetry as $(1a_u)^2(5a_g)^2\mathbf{(1b_g)^2(5b_u)^2}(6b_u)^2\mathbf{(6a_g)^2(2a_u)^2}(2b_g)^2(7a_g)^2$, whereas in ref 5, the configuration for the same species is $(1a_u)^2(5a_g)^2\mathbf{(1b_g)^2(5b_u)^2}(6b_u)^2\mathbf{(2a_u)^2(6a_g)^2}(2b_g)^2(7a_g)^2$. The same group claimed that this configuration of the outer valence shell, based on HF/6-311G**, is $(1a_u)^2(5a_g)^2\mathbf{(5b_u)^2(1b_g)^2}(6b_u)^2\mathbf{(2a_u)^2(6a_g)^2}(2b_g)^2(7a_g)^2$. The RHF/TZVP model in the present work indicates that in the one-particle description the outer valence shell configuration (X^1A_g) with C_{2h} symmetry is

$$(1a_u)^2(5a_g)^2(5b_u)^2(1b_g)^2(6b_u)^2(2a_u)^2(6a_g)^2(2b_g)^2(7a_g)^2 \quad (1)$$

which is confirmed by the RHF/aug-cc-pVTZ calculations conducted in present work. However, it is also noted that both the DFT related methods, DFT-BP/TZVP and B3LYP/TZVP, give the reversed orbital symmetry order of the HOMO and the next HOMO (NHOMO) as $2b_g$ and $7a_g$, respectively, reflecting changes of the orbital symmetry (with respect to the principal C_2 rotational axis of *n*-butane) as a result of energy ordering. This problem can be resolved with the help of orbital MDs, which will be discussed in the later sections in detail.

Figure 1 plots the valence orbital energies of *n*-butane (X^1A_g) against the orbital energy ordering. The orbital energies are compared among RHF/TZVP, DFT-BP/TZVP, and B3LYP/TZVP in the present work, with HF/6-311G** and 1p-GF/ADC-(3)/6-311++G** theoretical data.[3] The experimental outer valence binding energies[24] are also presented in this figure as a reference. Strictly speaking, experimental binding energies can only be approximated by orbital energies under the one particle description, which neglects the pair electron correlation and orbital relaxation effects in the ion wave functions. That is, Koopman's theorem[25] is only an approximation for binding energies in the HF theory in the single determinant SCF description. In DFT models, there does not exist such a simple relationship between the orbital energies and the binding energies. However, the orbital energies can be obtained by the Janak theorem[26] which defines the Kohn−Sham orbital energies as the first derivatives of the total energy with respect to the orbital occupation numbers (n_i); that is, the distribution of n_i that minimizes the total energy gives the orbital energy ϵ_i. Only the first binding energy can be approximated by the orbital energy of HOMO with half electron occupancy ($n = 1/2$).[27]

It is noted that the experimental binding energies of *n*-butane are not unambiguous with respect to the orbital symmetry, except for the inner valence MOs of *n*-butane. The HeI photoelectron spectra (PES)[24] gave reliable outer valence MO

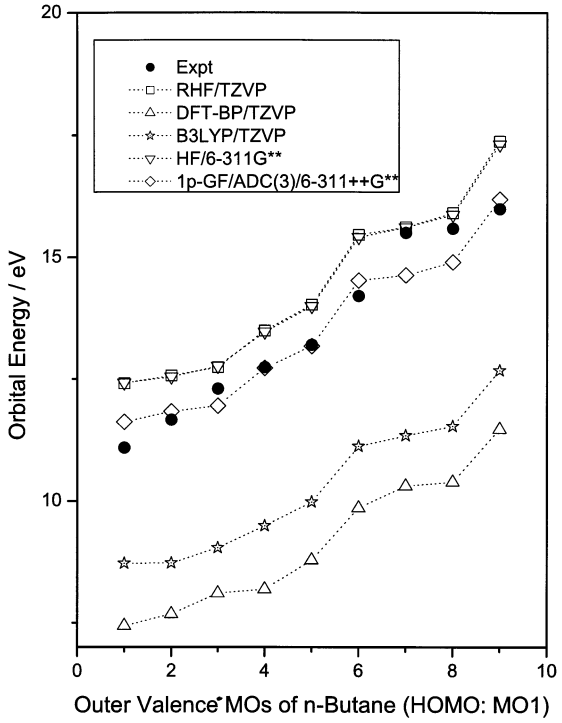

Figure 1. Outer valence orbital energy diagram of *n*-butane calculated using quantum mechanical methods of RHF/TZVP, B3LYP/TZVP, and DFT-BP/TZVP, together with experiments and other calculations.

energies but only energies. The individual MO symmetry assignment of *n*-butane was assisted by the HF/4-31G[24] calculations based on a point group symmetry of C_s (the symmetry of the global energy minimum structure of *n*-butane is C_{2h}, instead). Hence, the orbital symmetry in the HeI PES experiment relies on the HF/4-31G calculation and its orbital energy ordering and configuration. As indicated before, the ground state configuration for *n*-butane is not the same as the configuration given by the HF/4-31G model.[24] Consequently, PES cannot directly map a particular MO with its binding energy to its orbital wave function and therefore the orbital identification. The EMS experiment is able to directly map the orbital binding energies into its own orbital MDs (therefore, the orbital identification, at least to the fully resolved MOs). However, as the EMS technique is limited by its resolution at present and the outer valence shell of *n*-butane is unresolved, the observed orbital binding energies to its identified orbital wave functions of *n*-butane are determined unambiguously by experiment only for the inner valence shell.

III. Resolved Outer Valence Orbital MDs: Beyond Experiment

The EMS cross section for randomly orientated molecules is given by[10]

$$\sigma = K \int \mathrm{d}\Omega \, |\langle \Pi \, \Psi_f^{N-1} | \Psi_i^N \rangle|^2 \quad (2)$$

where K is a kinematical factor which is essentially constant in the experimental arrangement, Ψ_f^{N-1} and Ψ_i^N are the electronic many-body wave functions for the final ion *f* and the target molecular *i* ground electronic states, and Π is the momentum of the target electron at the instant of ionization. The $\int \mathrm{d}\Omega$ averages over molecular orientations. The basic theoretical approximations are the Born−Oppenheimer approximation, one-electron approximation (one particle description) for the target

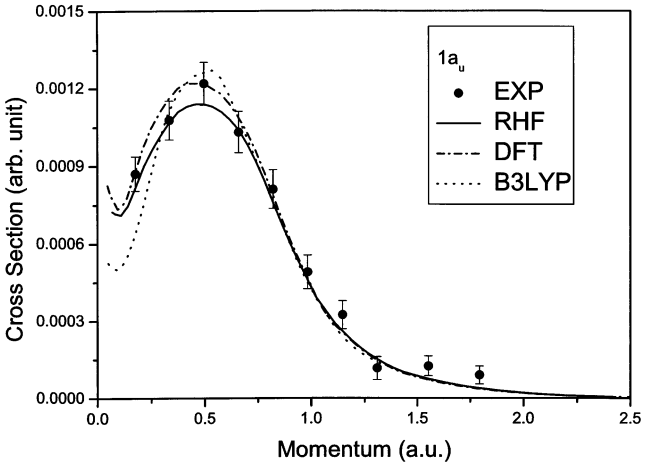

Figure 2. Comparison of the orbital MDs of $1a_u$ simulated using the quantum mechanical methods and the EMS experiment.

and ion wave functions, and the plane-wave impulse approximation (PWIA).[10]

The overlap of the initial and final electronic wave functions is a one-electron quantity known as the Dyson orbital. It can be approximated by an MO, $\psi_j(\Pi)$, using the same one-particle model for the target and ion. Equation 2 reduces to

$$\sigma = K S_j^{(f)} \int \mathrm{d}\Omega \, |\psi_j(\Pi)|^2 \qquad (3)$$

where the spectroscopic factor $S_j^{(f)}$ is the probability of one-hole configuration j being in the ion wave function Ψ_f^{N-1}.[28]

The simulation was set up to reflect the experimental EMS conditions.[5] Briefly, the energies of the two outgoing electrons A and B are equal, and the polar angle is $\theta = 45°$ with respect to the direction of the incident electron beam. The total energy (sum of the energies of A and B) is 1200 eV. The finite spectrometer acceptance angles are $\Delta\theta = \pm 0.6°$ and $\Delta\phi = \pm 1.2°$. Hence, the relationship between the azimuthal angle ϕ and the target electron momenta Π is given by[19]

$$\Pi = \left[(2\Pi_A \cos\theta - \Pi_0)^2 + 4\Pi_A{}^2 \sin^2\theta \sin^2\left(\frac{\phi}{2}\right)\right]^{1/2} \qquad (4)$$

A typographical error of this equation in ref 3 is noticed. Here $\theta = 45°$, $\Pi_A = 6.64077$ au and $\Pi_0 = 0.271105(1200 + \mathrm{IP})^{1/2}$ au[3]

The chemically most significant outer valence MOs including the frontier MO (HOMO) are not fully resolved in the experiment (except for MO $1a_u$).[5] The nine outer valence MOs of *n*-butane can be divided into three groups: (i) the experimentally resolved orbital $1a_u$, (ii) the experimentally partly resolved but unambiguously decomposable orbital clusters of $5a_g + 5b_u + 1b_g$ and $6b_u + 2a_u$, and (iii) the most complex three outermost orbitals of $6a_g + 2b_g + 7a_g$.

A. Orbital Based XC-Energies Assessment. Orbital MDs can be used to assess the anisotropy of the orbital wave function of a molecule and the quality of the orbital dependent XC energies represented by the QM models. In Figure 2, the simulated orbital MDs of $1a_u$ are displayed against the experimentally observed cross sections. As expected, the orbital MDs are nearly identical in the larger momentum region of $\Pi > 0.75$ au but the QM orbital MDs split as the momentum decreases. All models indicate a local minimum of the orbital cross sections with the DFT related models exhibiting the minimum to a larger extent. The B3LYP orbital MDs clearly exhibit a larger gradient in orbital MDs in the region of $\Pi < 0.25$ au and display a larger MD peak at $\Pi \approx 0.50$ au than both of the RHF and DFT-BP orbital MDs. On the other hand, the orbital MDs simulated by the RHF/TZVP and DFT-BP/TZVP models are closer to the experiment than the B3LYP orbital MDs in the region of $\Pi < 0.25$ au, so that this QM pair is of similar quality in predicting the orbital anisotropy. However, it is difficult to assess the quality of these models in the MD peak region (where the models diverge) unless more experimental data in this region are provided, as the orbital MD discrepancies between these QM models are within the experimental error bars. The lack of sufficient experimental data in the region of $\Pi < 0.25$ au also makes it difficult to assess the large orbital MD discrepancies given by the QM models. Hence, the present work indicates that more intense data in the region of $\Pi \approx 0.50$ au are needed for new EMS experiment of this species.

B. Unambiguously Decomposable Orbital Clusters of $5a_g + 5b_u + 1b_g$ and $6b_u + 2a_u$. Figures 3 and 4 give the orbital MDs of the two unambiguously decomposable orbital clusters containing five outer valence MOs, which are partly resolved by the experiment.[5] Figure 3a gives the partially resolved clustered MDs of $5a_g + 5b_u + 1b_g$, superpositioned by the orbital MDs simulated from individual QM models against the experiment. All models are able to produce the major features regarding turning points (sign changes in gradient) in the small momentum region of less than $\Pi < 1.0$ au. The QM orbital MDs are almost indistinguishable in the large momentum region of $\Pi > 1.0$ au and agree well with the experiment. As the large momentum region corresponds to small distances in the configuration space, this indicates that the QM models are reliable in the prediction of electronic structural information at the vicinity of the molecular equilibrium structure. The QM orbital MDs start to split as the momentum moves to the left-hand side, but all are well within the experimental error bars until the momentum hits 0.50 au. The orbital MD splitting among the quantum mechanical methods and the experiment becomes apparently large in the region of $\Pi < 0.25$ au as indicated in Figure 3a. Similar to what was found in MO $1a_u$ of Figure 2, the B3LYP orbital MDs split from the orbital MDs generated by the other models in the small region of $\Pi < 0.25$ au and largely underestimate the orbital anisotropy in this region. The RHF and DFT-BP pair exhibits similarly quality and demonstrates better agreement with the experimental orbital cross sections than the B3LYP model, even though the former also underestimates the orbital anisotropy in the same region. Therefore, RHF and DFT-BP models will be able to provide a more appropriate description for this orbital cluster in the long range.

Although the clustered MOs simulated by different models agree well each other and also with the experiment as demonstrated in Figure 3a, this does not guarantee a well behavior of the individual orbital MDs generated from the same models. The discrepancies between the models are orbital and symmetry dependent, which provides an excellent base to make comparison on the quality of the QM models involved. Figure 3, parts b−d, shows the individual orbital MDs for the $1b_g$, $5b_u$, and $5a_g$ MOs, respectively. The orbital MDs of the $1b_g$ and $5a_g$ MOs (Figure 3, parts b and d) exhibit a similar p-like feature as can be expected from the clustered orbital MDs in Figure 3a. It is a surprise that the individual QM models behave so differently in presenting the orbital MDs of the $5b_u$ MO (Figure 3c). This orbital MDs indicate a significant *s*-AO and *p*-AO mixed character. Such important bonding information has been masked and entirely invisible in the unresolved experimental MDs (Figure 3a). However, all QM models in Figure 3c produce

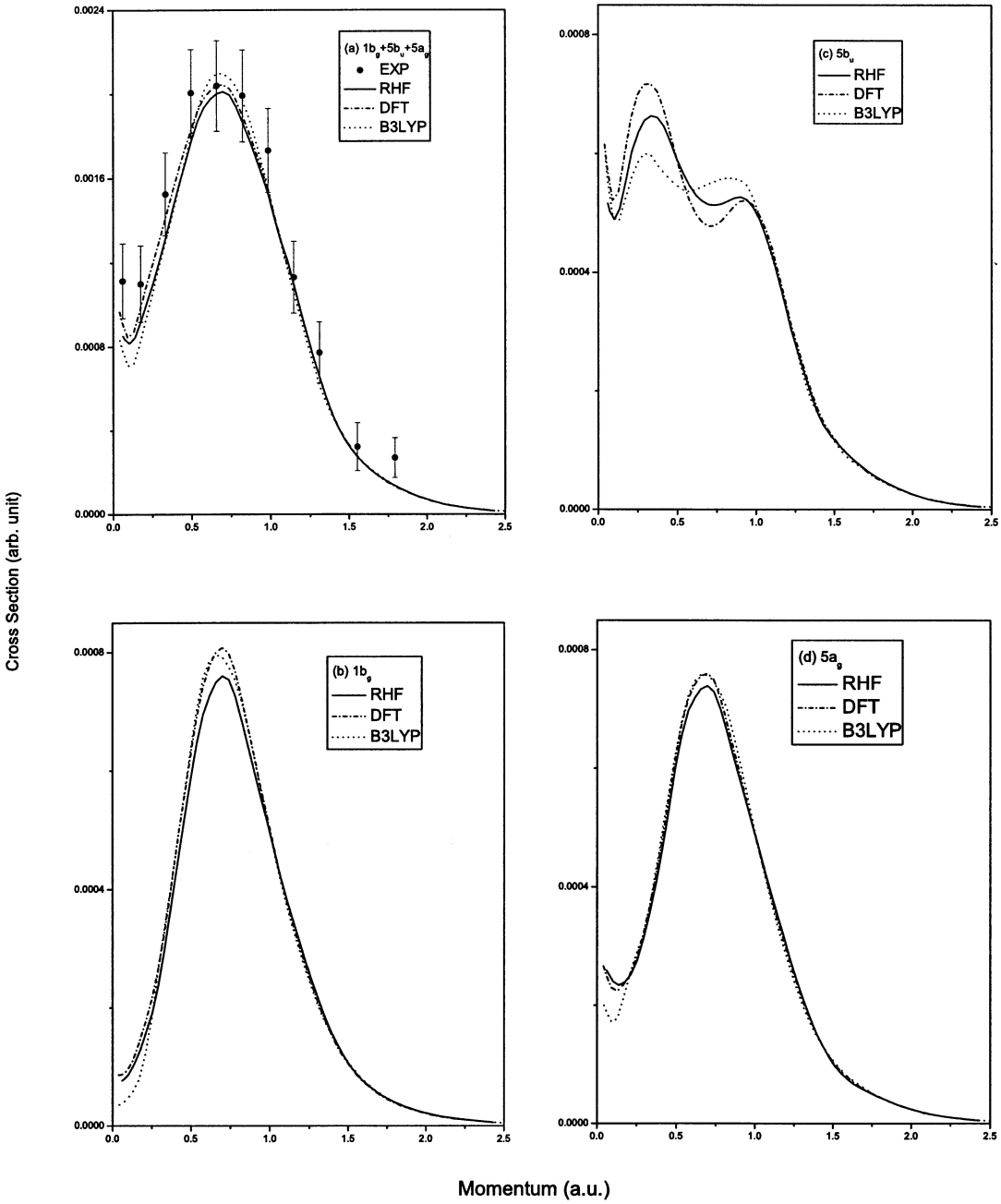

Figure 3. Orbital MDs of the decomposed three outer MOs: (a)$1b_g + 5b_u + 5a_g$, (b) $1b_g$, (c) $5b_u$, and (d) $5a_g$.

the same major features but vary in the MD amplitudes. The RHF/TZVP and DFT-BP/TZVP orbital MDs exhibit large deviations with the DFT-BP/TZVP orbital MDs varying in particularly large amplitudes. This may imply that the orbital dependent exchange (X) energy functional of the DFT-BP underestimates the X energy or the electron correlation (C) functional overestimates the C energy or vice versa. Consequently, caution must be taken when applying different QM models in the study of the chemical reaction in the long range such as bond formation and break, due to inappropriate XC energy and orbital anisotropy.

The orbital MDs of two p-like orbitals $1b_g$ and $5a_g$ (Figure 3, parts b and d) are reproduced well by the QM models except for the cross section peak region of [0.5, 0.8] au and the small momentum region of less than 0.25 au. In the case of $1b_g$, the B3LYP orbital MDs underestimate the orbital anisotropy in the region of $\Pi < 0.25$ au but become closer to the other models when the momentum increases and nearly overlap with the DFT-BP/TZVP orbital MDs. The DFT-BP and RHF orbital MDs agree well in the small momentum region until 0.50 au where they largely split as illustrated in Figure 3b. The behavior of MO $5a_g$ in Figure 3d is similar to that of MO $1b_g$ except that (i) this MO exhibits a local minimum at $\Pi \approx 0.15$ au and (ii) the QM orbital MDs split into two groups of B3LYP/TZVP as well as RHF/TZVP and DFT-BP/TZVP in the region of $\Pi <$ 0.50 au but being repaired in the peak region of [0.5, 1.0] au into B3LYP and DFT-BP as well as RHF. This implies that the B3LYP model contains inappropriate XC energy for this MO in the small Π region, but this is improving as Π increases. Superposition of MOs $1b_g$, $5b_u$, and $5a_g$ gives an sp-hybridized (strong s- and p-AO coupling) clustered MO from a strong p-like MO ($1b_g$), an s-AO and p-AO mixed MO (weak s- and p-AO coupling, $5b_u$) and a hybridized MO ($5a_g$). The orbital MDs of the $5b_u$ MO behave like a transition made between the $1b_g$ and $5a_g$ MOs. Figure 3, parts a−d, clearly demonstrates how the

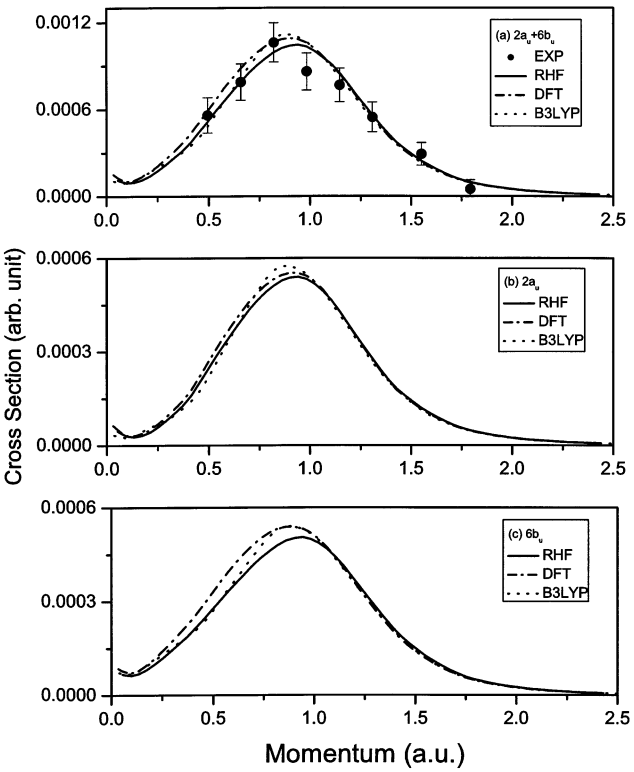

Figure 4. Orbital MDs of the decomposed two outer MOs: (a) $2a_u + 6b_u$, (b) $2a_u$, and (c) $6b_u$.

MDs of a group of very different individual orbitals could cause valuable bonding information loss.

The decomposition of clustered MOs of $6b_u$ and $2a_u$ is rather straightforward. Figure 4a−c portrays the two p-like orbitals, collectively (part a) and respectively (parts b and c). In these MOs, all of the models agree well in general with only small shifts upward in the MD peak region. The agreement indicates that all of these models are able to independently predict the reliable orbital anisotropy. Inclusion of the XC energy in the QM models does not make apparent improvement to the orbital MDs with the experiment. Further examining the symmetry of the $2a_u$ and $6b_u$ MOs, they are symmetric (a) and anti-symmetric (b) with respect to the rotational C_2 operation. As a consequence, MO $2a_u$ is dominated by the carbon $2p_z$ AOs, whereas MO $6b_u$ is dominated by the carbon $2p_x$ or $2p_y$ AOs. Figure 4 confirms such a bonding mechanism by indicating that the $2a_u$ and $6b_u$ MOs are both strongly p-like MOs. As the experimental orbital MDs did not sample the cross sections with sufficiently low momenta to reveal the local minimum at approximately $\Pi = 0.15$ au,[5] the present simulation suggests further EMS experiments with larger concentration of the data in the low momentum region of these MOs.

C. Analysis of the Complex Outermost Orbitals of $7a_g + 2b_g + 6a_g$. If it is a surprise that the bonding information of the s- and p- mixed MO $5b_u$ is masked by the unresolved clustered MOs of $1b_g + 5b_u + 5a_g$ collectively in Figure 3a, it can be astonishing if one sees the complexity of the three outermost MOs. The HOMO, NHOMO, and MO3 agree "well" collectively to the unresolved experiment. Figure 5a compares the three clustered orbital MDs simulated using the QM models with available experimental cross sections. The comparison shows that the clustered MOs with a strong s-AO and p-AO mixed character and that a "good" agreement with the experiment has been achieved, except for the DFT-BP/TZVP orbital MDs which exhibit small deviation in the region of $\Pi < 1.00$ au. The RHF and B3LYP models provide consistent results in almost the entire momentum region, but B3LYP further produces the turning point at $\Pi \approx 0.15$ au, as indicated in the EMS experiment.[5] Hence, from Figure 5a, we may conclude that these QM models produce electronic calculations with similar quality and approximately the same orbital XC energy and anisotropy. Similar observation and conclusions can also be made from the analysis of the simulated orbital MDs of the third MO $6a_g$ as displayed in Figure 5b, where the QM orbital MDs agree very well in the entire momentum region with B3LYP being slightly better in the region of less than 0.10 au. Despite the subtle difference, it indicates that this orbital is not sensitive with respect to electron correlation energy and orbital anisotropy so that the HF wave function has sufficient accuracy to predict it's orbital MDs.

The most interesting and challenging issue of the clustered MOs is the HOMO (MO1) and NHOMO (MO2) of *n*-butane calculated using these QM models. It has been noted in the previous section that the orbital symmetries of the HOMO and NHOMO are different using RHF and DFT models. In RHF/TZVP, the orbital symmetries of HOMO and NHOMO are $7a_g$ and $2b_g$, respectively, whereas the symmetries using B3LYP/TZVP and DFT-BP/TZVP are $2b_g$ for HOMO and $7a_g$ for NHOMO. Figure 5, parts c and d, gives the orbital MDs for MO2 and MO1, respectively, simulated using those QM models. At the first glance, the orbital MDs of MO1 and MO2 seem significantly different as a result of ab initio and DFT calculations. There is no further experimental information to indicate which model gives the correct orbital energy ordering for these individual MOs. However, such information beyond the experiment can be obtained from theoretical molecular spectroscopy and the point group symmetry. Further analyzing Figure 5a−d, it is clear that all models agree on the MO3 with an a_g symmetry of a strong s-like with some p-like contribution, which implies that the HOMO with also an a_g symmetry may have the orbital MDs with a similar feature as that in Figure 5b. The RHF/TZVP calculation indicates that the NHOMO is dominant by contribution between the carbon $2p_x$ and $2p_y$ AOs so that the NHOMO ought to be p-like. The orbital MDs of the RHF/TZVP in Figure 5d possess the appropriate MO symmetry of a_g for the HOMO, whereas the p-like orbital MDs in the same figure simulated by the B3LYP/TZVP and DFT-BP/TZVP models belong to the NHOMO $2b_g$. Figure 5, parts e and f, presents the MDs of the HOMO and NHOMO with "appropriate" orbital symmetries. The QM models agree very well on the NHOMO of $2b_g$ with small discrepancies in the cross section peak region and small momentum region.

IV. Assessment of the QM Models Using Orbital MDs

A reason which causes the orbital symmetry alternation between the HOMO and NHOMO in the B3LYP/TZVP and DFT-BP/TZVP models stems from the nature of ab initio and DFT models. Here, B3LYP is considered as a DFT method. The electronic Schrödinger equation on which the RHF is based focuses on the total energy of the molecule. By obtaining the lowest energy (in variational methods), one assumes that the associated wave function yields the electron distribution of the ground electronic state. In the DFT theory, the Schrödinger equation is "bypassed" and attention is focused on the electron density from which many desired properties including energy can be derived directly. Perhaps one of the largest noticeable differences in the DFT theory is that the number of electron occupancy, n_i, does not need to be an integer and $0 \leq n_i \leq 1$.[27] This causes the 18th MO in *n*-butane to also possess negative

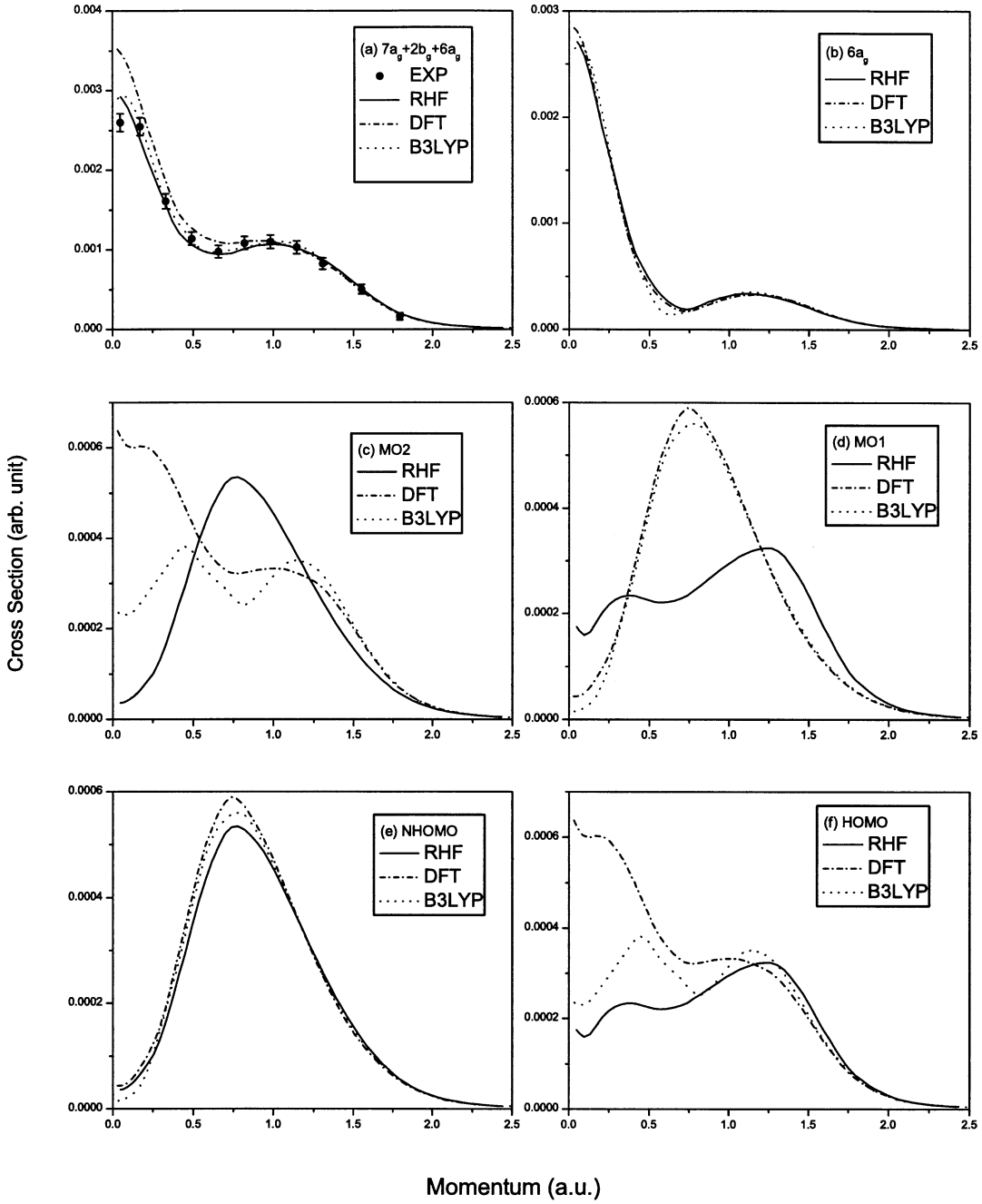

Figure 5. Decomposed valence orbital MDs of the outermost valence MO clusters: (a)$7a_g + 2b_u + 6a_g$, (b) MO3 ($6a_g$), (b) MO2, and (c) MO1, together with the MOs with "appropriate" orbital symmetries of NHOMO ($2b_u$) (d) and HOMO ($7a_g$) (e).

orbital energy from the B3LYP/6-311++G** calculations.[3] Therefore, strictly speaking, the "HOMO" of *n*-butane as discussed in ref 3 using B3LYP/6-311++G** calculations is in fact the MO of the species with the second highest negative orbital energy. This fact indicates that the 1p-GF/ADC(3)/6-311++G** orbital energies and the B3LYP/6-311++G** orbital wave functions are not on the one-to-one base and do not have direct connections. The parametrized and approximated XC functionals of the DFT methods and wave function imperfection may contribute to the energy alternation of the outermost valence MOs. Only an energy splitting of 0.01 eV between HOMO (8.72 eV) and NHOMO (8.73 eV) given by the B3LYP/TZVP model, and of 0.24 eV between HOMO (7.44 eV) and NHOMO (7.68 eV) are observed from the DFT-BP/TZVP model. As indicated in Figure 5e, for the p-like orbital MDs of NHOMO, $2b_g$, all of the QM models agree quite well. Agreement from different models on the MDs of the next highest occupied MO also implies that the orbital electron XC energy to this particular orbital anisotropy is insignificant.

The significantly different orbital MDs of HOMO ($7a_g$), as exhibited in Figure 5f given by the QM models are somehow unexpected. Despite the orbital symmetry difference in HOMO and NHOMO, given by ab initio and DFT models, two of the QM models, namely, RHF and B3LYP, agree quite well collectively with each other and with the experiment (Figure 5a). Although the QM models display the HOMO a strong s-AO and p-AO interacted MO, the DFT-BP/TZVP model gives a MO with strong s-like with some p-AO character. Based on the clustered experimental MDs of Figure 5a and molecular orbital theory, it can be concluded that the DFT-BP/TZVP model produces the inappropriate orbital MDs for the *n*-butane HOMO ($7a_g$). The reasons are as follows. The orbital MDs in Figure

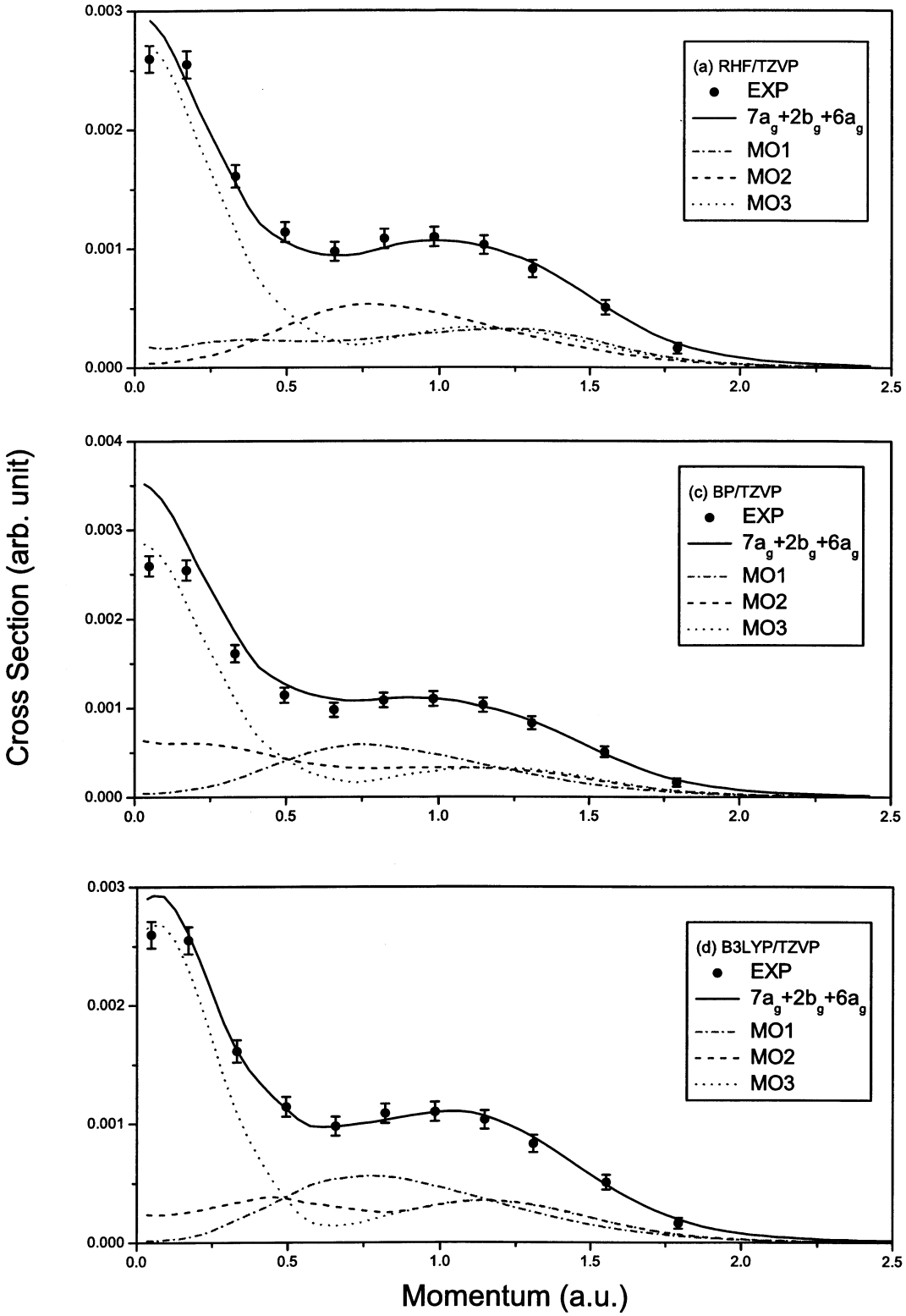

Figure 6. Decomposition of the clustered outermost valence orbital MDs of *n*-butane using the quantum mechanical models: (a)RHF/TZVP, (b) DFT-BP/TZVP, and (c) B3LYP/TZVP.

5a strongly suggest that DFT-BP/TZVP overestimates the orbital MDs in the small momentum region of less than 1.0 au, though unresolved and as a collection of three orbitals $7a_g + 2b_g + 6a_g$. The orbital MD amplitudes of both HOMO and NHOMO are nearly five times weaker than the MDs of MO3, $6a_g$. However, the nearly indistinguishable orbital MDs of this MO ($6a_g$) given by the QM models make it possible to assess the impact of HOMO and NHOMO. Nevertheless, the HOMO is a frontier MO of *n*-butane, and it must represent one of the C−H or C−C bonds. None of the C−H bonds or outer valence C−C bonds can be dominated by two s-AOs. Instead, those bonds can be only formed either by a hydrogen (or carbon) s-AO and a carbon 2p-AO (s- and p-mixed MOs) or two carbon 2p-AOs (p-like MOs). The orbital MDs simulated by RHF/TZVP and B3LYP/TZVP confirm the s- and p-mixed HOMO. The strong s-like MO predicted by the DFT-BP/TZVP model is, therefore,

inappropriate. As the B3LYP model is a hybrid functional, which defines the exchange functional as a linear combination of Hartree−Fock, local, and gradient-corrected exchange terms, it is concluded that the exchange-energy functional[11] in the DFT-BP model may be incorrect for the HOMO of *n*-butane.

Figure 6a−c demonstrates how a set of three very different orbital MDs can collectively produce nearly the same behavior as unresolved MOs. Parts a−c of Figure 6 each present three individual orbital MDs of the HOMO, NHOMO, MO3, and their superpositioned MDs, using the QM models of RHF/TZVP, DFT-BP/TZVP, and B3LYP/TZVP. This figure indicates that the DFT-BP/TZVP model gives a "reasonably" good agreement with the unresolved experiment in the small momentum region which is merely due to the large MD amplitudes of MO3 in this region, which makes the unphysical behavior of its HOMO "invisible" as a result of the relatively weak spectroscopic strength of the HOMO. The clustered orbital MDs of the three outermost MOs also cause important orbital bonding information losses.

V. Conclusions

Outer valence molecular orbitals of normal butane in the ground electronic state (X^1A_g), which possesses the global minimum structure on the potential energy surface with a C_{2h} point group symmetry, are studied using different QM models, together with the plane wave impulse approximation (PWIA). The present work provides individual outer valence orbital MD simulation and has demonstrated that different QM models indeed result in significantly different orbital MDs of the chemically most important MOs such as the HOMO and NHOMO, although all models produce very good agreement with experiment on the partly resolved clustered MOs and other valence MOs. The orbital momentum distributions of HOMO and NHOMO in *n*-butane are analyzed and resulted in unambiguous information of these orbitals in momentum space in the first time.

The present work largely adds to the existing knowledge of the bonding mechanism of normal butane in the ground electronic state on the individual orbital base. The agreement between the simulations and the available experiment provides insight understanding of the QM models, in particular, orbital wave function anisotropy and the inclusion of orbital dependent exchange-correlation energies in the DFT methods. DFT methods are very attractive as they provide a more anisotropic orbital wave function of the molecular species than many of the ab initio methods. However, as DFT methods are less well understood than the RHF method, an appropriate use of certain DFT methods with a basis set requires more research effort in order to ensure that the models employed are proper to a particular species.

Acknowledgment. The author acknowledges the Australian Partnership for Advanced Computing (APAC) for using the Compaq SC AlphaServer Cluster National Facilities and the HPCCC group of CSIRO for high performance computer resources. Professor Ian E. McCarthy is acknowledged for providing the original AMOLD codes and Professor Wenning Pang for the *n*-butane EMS experimental data.

References and Notes

(1) Rauk, A.; *Orbital Interaction Theory of Organic Chemistry*, 2nd ed.; Wiley-Interscience: New York, 2001.

(2) Allinger, N. L.; Fermann, J. T.; Allen, W. D.; Schaefer, H. F., III. *J. Chem. Phys.* **1997**, *5143*, 106.

(3) Deleuze, M. S.; Pang, W. N.; Salam, A.; Shang, R. C. *J. Am. Chem. Soc*. **2001**, *4049*, 123.

(4) Pang, W. N.; Shang, R.; Gao, N.; Zhang, W.; Gao, J.; Deng, J.; Chen, X.; Zheng, Y. *Phys. Lett. A* **1998**, *203*, 248.

(5) Pang, W. N.; Gao, J. F.; Ruan, C. J.; Shang, R. C.; Trofimov, A. B.; Deleuze, M. S. *J. Chem. Phys.* **2000**, 8043, 112.

(6) Wang, F.; Downton, M. submitted for publication.

(7) Downton, M.; Wang, F. submitted for publication.

(8) Deng, J. K.; Li, G. Q.; He, Y.; Huang, J. D.; Deng, H.; Wang, X. D.; Wang, F.; Zhang, Y. A.; Ning, C. G.; N. Gao, F.; Chen, X. J.; Zheng, Y. *J. Chem. Phys.* **2001**, *882*, 114.

(9) Deng, J. K.; Li, G. Q.; Huang, J. D.; Deng, H.; Wang, X. D.; Wang, F.; He, Y.; Zhang, Y. A.; Ning, C. G.; Gao, N. F.; Wang, Y.; Chen, X. J.; Zheng, Y.; Brion, C. E. *Chem. Phys. Lett.* **1999**, *134*, 313.

(10) McCarthy, I. E.; Weigold, E. *Rep. Prog. Phys.* **1991**, *789*, 54.

(11) Becke, A. D. *J. Chem. Phys.* **1988**, *88*, 2574.

(12) Perdew, J. P. *Phys. Rev. B* **1986**, *33*, 8822.

(13) Godbout, N.; Salahub, D. R.; Andzelm, J.; Wimmer, E. *Can. J. Chem.* **1992**, *70*, 560.

(14) Winkler, D. A.; Michalewicz, M. T.; Wang, F.; Brunger, M. J. *J. Phys. B: At. Mol. Phys.* **1999**, *3239*, 32.

(15) Adcock, W.; Brunger, M. J.; McCarthy, I. E.; Michalewicz, M. T.; von Niessen, W.; Wang, F.; Weigold, E.; Winkler, D. A. *J. Am. Chem. Soc.* **2000**, *3892*, 122.

(16) Wang, F.; Mackenzie-Ross, H.; Winkler, D. A.; McCarthy, I. E.; Campbell, L.; Brunger, M. J. *J. Comput. Chem.* **2001**, *1321*, 22.

(17) Mackenzie-Ross, H.; Brunger, M. J.; Wang, F.; Adcock, W.; Trout, N.; Winkler, D. A. *J. Electron Spectrosc. Relat. Phenom.* **2002**, *389*, 123.

(18) Mackenzie-Ross, H.; Brunger, M. J.; Wang, F.; Adcock, W.; Maddern, T.; Newell, W. R.; McCarthy, I. E.; Weigold, E.; Appelbe, W.; Winkler, D. A. *J. Phys. Chem. A* **2002**, *9573*, 106.

(19) Nixon, K.; Wang, F.; Campbell, L.; Maddern, T.; Winkler, D. A.; Gleite, R.; Loeb, P.; Weigold, E.; Brunger, M. J. *J. Phys. B: At. Mol. Phys.* **2003**, *3155*, 36.

(20) Schmidt, M.; Baldridge, K.; Boatz, J.; Elbert, S.; Gorden, M.; Jensen, J.; Koseki, S.; Matsunaga, N.; Nguyen, K. A.; Windus, T. L.; Dupuis, M.; Montgomery, J. A. *J. Comput. Chem.* **1993**, *1347*, 14.

(21) Andzelm, J.; Wimmer, E. *J. Chem. Phys.* **1992**, *1290*, 96.

(22) Komorniki, A.; Fitzgerald, G. J. *J. Chem. Phys.* **1993**, *1398*, 98.

(23) Wang, F.; McCourt, F. R. W.; Le Roy, R. J. *J. Chem. Phys*. **2000**, *98*, 113.

(24) Kimura, K.; Katsumata, S.; Achiba, Y.; Yamazaki, T.; Iwata, S. *Handbook of HeI Photoelectron Spectra of Fundamental Organic Molecules*; Japan Scientific Society: Tokyo, 1981.

(25) Koopmans, T. *Physica* **1933**, *104*, 1.

(26) Janak, J. F. *J. Chem. Phys.* **1978**, *7165*, 18.

(27) Parr, R. G.; Yang, W. *Density Functional Theory of Atoms and Molecules*; Oxford Science Publications: New York, 1989.

(28) Weigold, E.; McCarthy, I. E. *Electronic Momentum Spectroscopy*; Klumer Academic/Plenum Pbulishers: New York, 1999.